ORIGINAL CONTRIBUTION

Graphene oxide incorporated alginate hydrogel beads for the removal of various organic dyes and bisphenol A in water

Lu Gan[1] · Hui Li[1] · Liwei Chen[2] · Lijie Xu[2] · Jie Liu[3] · Aobo Geng[1] · Changtong Mei[1] · Songmin Shang[4]

Abstract
In the present study, we described a facile preparation of graphene oxide incorporated alginate hydrogel beads (SA/GO) and applied them in adsorbing organic pollutants in aqueous media. The results show that the incorporation of graphene oxide obviously decreased the pore size and swelling ratio of the hydrogel beads. The existence of the GO also significantly enhanced the adsorption capability of the SA/GO beads to various organic dyes, including heterocyclic dye, indigo dye, anthraquinone, and azo dye. Besides, the SA/GO beads show promising adsorption capability to the bisphenol A (BPA), a toxic chemical which could cause endocrine disruption. The adsorption isotherm and kinetic of the SA/GO beads were also studied in detail. The present study indicates that the SA/GO beads are a type of effective absorbent for various organic pollutants which have the potential to be applied in water purification fields.

Keywords Graphene oxide · Alginate bead · Organic dyes adsorption · BPA removal · Kinetic

Introduction

Sodium alginate (SA), a linear binary heteropolymer, is a kind of natural polysaccharide being composed of α-L-guluronate units and β-D-mannuronate units which are linked through varying ratios [1–3]. The non-toxicity, biocompatibility, and ease of gelling from hydrophilic sodium alginate to aqueous insoluble calcium alginate through ionic crosslinking enable the application of alginate gel in various fields such as drug release and wound healing [4–6]. Recently, the SA gel materials have received tremendous research interest since they show promising adsorbing affinity to numerous materials like

metal ions, antibiotics, and many organic pollutants in aqueous media, which make the alginate gel a desirable candidate in the application of water purification [7, 8].

On the other hand, the 2-D structured graphene-related materials and their derivatives have received numerous interests in a variety of research fields due to their unique properties [9, 10]. As a significant derivative, the graphene oxide (GO) has found tremendous applications in composites, electronics, catalysts, and water purifications [11–13]. The high surface area and the large amounts of functional groups like carboxyl groups, epoxy groups, and hydroxyl groups existed within the GO skeleton enable the GO with strong affinity to various organic and inorganic molecules [14]. Due to this reason, the GO is considered a desirable material for enhancing the adsorbing performance of hydrogel materials, and great efforts have been devoted to exploring the capability of the GO-based hydrogel materials for organic pollutant removal [15, 16].

In recent years, tons of organic dye wastewater have been discharged and caused serious environmental problems [17]. Many dyes and their degradation products are toxic, carcinogenic, which cannot be easily biodegraded naturally. More recently, the bisphenol A (BPA) also caused panic among human beings since it is viewed as an endocrine-disrupting chemical (EDC) which can interfere the reproduction and gene transformation of human and animals [18]. Thus, the

✉ Lu Gan
ganlu@njfu.edu.cn

1 College of Materials Science and Engineering, Nanjing Forestry University, Nanjing 210037, Jiangsu, People's Republic of China

2 College of Biology and the Environment, Nanjing Forestry University, Nanjing 210037, Jiangsu, People's Republic of China

3 School of Chemical Biology and Materials Engineering, Suzhou University of Science and Technology, Suzhou 215009, Jiangsu, People's Republic of China

4 Institute of Textiles and Clothing, The Hong Kong Polytechnic University, Hong Kong, People's Republic of China

removal of both organic dyes and BPA from water system is of extreme significance.

Based on the above facts, the SA/GO hydrogel beads were fabricated through ion-exchange gelling process. The structure of the hydrogel beads were characterized afterwards. The adsorbing capability of the fabricated beads was then investigated through removing various organic dyes, including heterocyclic dye, indigo dye, anthraquinone, and azo dye in aqueous media. Moreover, the BPA removal efficiency of the SA/GO hydrogel beads was also studied in detail. One issue which should be pointed out that although the adsorption behavior of the SA hydrogel composites has been studied through adsorbing different molecules, the adsorbed target are mainly ionic molecules, including metal cations and ionic molecules which are easily ionized in water [19, 20]. These ionized molecules can be adsorbed by SA/GO hydrogel more easily through ionic interactions. Few studies investigated the adsorption behavior of SA/GO hydrogel to non-ionic molecules. Furthermore, a number of studies have reported the promising adsorption capability of GO to the non-ionic molecules [21, 22]. Thus, the GO should be a promising functional filler to improve the adsorption capability of SA to the non-ionic molecules with small incorporation amount. Through studying the adsorption behavior of the SA/GO beads to BPA, the adsorption capacity of the SA/GO beads to non-ionic molecules could be clearly illustrated.

Experimental

Materials

Natural graphite powder was purchased from Aldrich (America). Sodium alginate (SA, viscosity 350–550 mPa s) was purchased from Beijing Yonge Water Biological Technology Co., Ltd. (China). Methylene Blue (MB), Rhodamine B (RhB), Vat Green 1 (VG1), and Methyl Orange (MO) were also purchased from Beijing Yonge Water Biological Technology Co., Ltd. (China), which represented for the heterocyclic dye, indigo dye, anthraquinone, and azo dye respectively in the present study. Bisphenol A (BPA, m.w. = 228, Purity ≥ 99%) was purchased from Aldrich (USA). The parameters of the chemicals to be adsorbed were listed in Table 1. Other reagents were of analytical grade and used as received without further purification. Deionized water (H$_2$O) was used exclusively in this study.

Preparation of SA/GO hydrogel beads

The GO was prepared from natural graphite powder using modified Hummer's method described elsewhere [23]. The SA/GO hydrogel beads with different GO mass contents were prepared using an ion-exchange gelling process as follows.

Certain amount of GO was first put into 10 mL of H$_2$O and sonicated for 2 h to obtain a uniform dispersion. At the same time, 1 g SA was dissolved in 50 mL of H$_2$O with continuous mechanical stirring until a transparent SA solution was obtained. The GO dispersion was added into the SA solution. After 2 h of sonication and 1 h of mechanical stirring, the homogeneous SA/GO-mixed dispersion was obtained. The SA/GO hydrogel beads were then formed by a ion exchange process through injecting the SA/GO dropwise into a calcium chloride solution (CaCl$_2$, 10 M), during which process the CaCl$_2$ solution was stirred gently with a magnetic stirrer to prevent bead agglomeration. Afterwards, the instantaneously formed hydrogel beads were placed in the CaCl$_2$ solution for another 4 h to complete the ion exchange process. The SA/GO beads with the GO mass contents of 0.5 and 1.0 wt% were finally obtained after being washed with H$_2$O for three times to rinse out the un-reacted ions. For comparison, pure SA hydrogel beads were also prepared with similar procedures.

Characterizations

The crystalline structure of the hydrogel beads was characterized by X-ray diffraction (XRD) which was conducted using a Rigaku Smartlab XRD instrument with the Cu Kα radiation source (1.54 Å). Fourier transform infrared (FT-IR) spectra were recorded by a Perkin Elmer 100 spectrophotometer. Scanning electron microscopy (SEM) was conducted by the JEOL SEM 6490. The hydrogel beads were freeze-dried and coated with a thin gold film before observation. The thermogravimetric analysis (TGA) was measured using a Mettler Toledo TGA/DSC 1 Simultaneous Thermal analyzer with the temperature increasing from 25 to 700 °C at a heating rate of 10 °C/min under air, and the flow rate was set at 50 mL/min.

Swelling test

The swelling ratio (SR, %) of freeze-dried hydrogel beads was immersed in 200 mL of H$_2$O for 24 h at 25 °C to reach the equilibrium. The SR was calculated as:
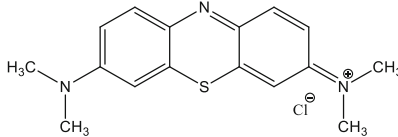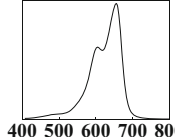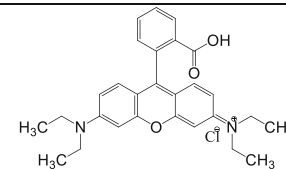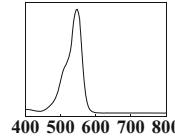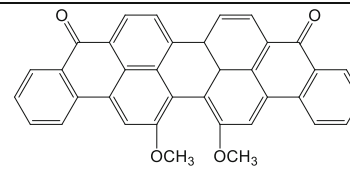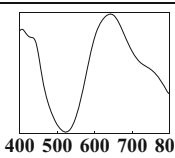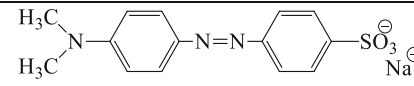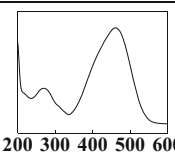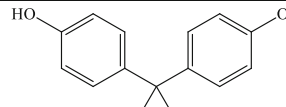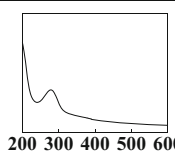
$$SR = \frac{(m_t - m_0)}{m_0} \times 100 \tag{1}$$

where m_0 is the mass weight of the freeze-dried hydrogel beads and m_t is the mass ratio of the swollen beads.

Dye adsorption of the hydrogel beads

In a vial, 10 mg of freeze-dried hydrogel beads were immersed in 25 mL of dye solution (100 mg/L for MB and RhB; 50 mg/L for VG1 and MO). The vial was placed in a thermostatic shaker with water bath (25 °C). After a certain period of time,

Table 1 Parameters of the dyes and bisphenol A used in the present study

Chemicals	Structure Formula	UV-vis spectra Max. Absorb.(nm)
Methylene Blue (MB) (Heterocyclic dye)	$C_{16}H_{18}ClN_3S$	400 500 600 700 800 665
Rhodamine B (RhB) (Basic dye)	$C_{28}H_{31}ClN_2O_3$	400 500 600 700 800 550
Vat Green 1 (VG1) (Anthraquinone dye)	$C_{36}H_{22}O_4$	400 500 600 700 800 640
Methyl Orange (MO) (Azo dye)	$C_{14}H_{14}N_3NaO_3S$	200 300 400 500 600 462
Bisphenol A (BPA)	$C_{15}H_{16}O_2$	200 300 400 500 600 275

the solution samples were taken out, and the amount of the absorbed dyes by the beads was measured by a UV-Vis spectroscopy (Lambda-18 UV-visible spectrometer). The absorbance numbers at 665, 550, 640, and 462 cm^{-1} corresponding to the maximum absorption of MB, RhB, VG1, and MO were used to determine the concentration variation of the dyes, respectively. After measuring, the solutions were placed back into the bottle at once to keep the total volume of the solution constant. The adsorption amount of the dyes was calculated using the following equation:

$$q_e = \frac{(C_0 - C_t)V}{m} \qquad (2)$$

where q_e is the absorption amount of the dyes on the hydrogel beads (mg/g), C_0 is the initial dye concentration (mg/L), C_t is

the dye concentration at equilibrium (mg/L), V is the volume of the dye solution (L), and m is the mass weight of the hydrogel beads used (g). Each absorption cycle was duplicated with an average result value. The effect of pH value to the adsorption amount of the dyes was also tested using the above method.

The effect of hydrogel beads amount to the dye adsorption percentage and the effect of the dye concentration to the adsorption capacity of certain amount of beads were also investigated using similar method as above. The removal of the dyes was calculated using the following equation:

$$\text{Removal}, \% = \frac{C_0 - C_t}{C_0} \times 100 \qquad (3)$$
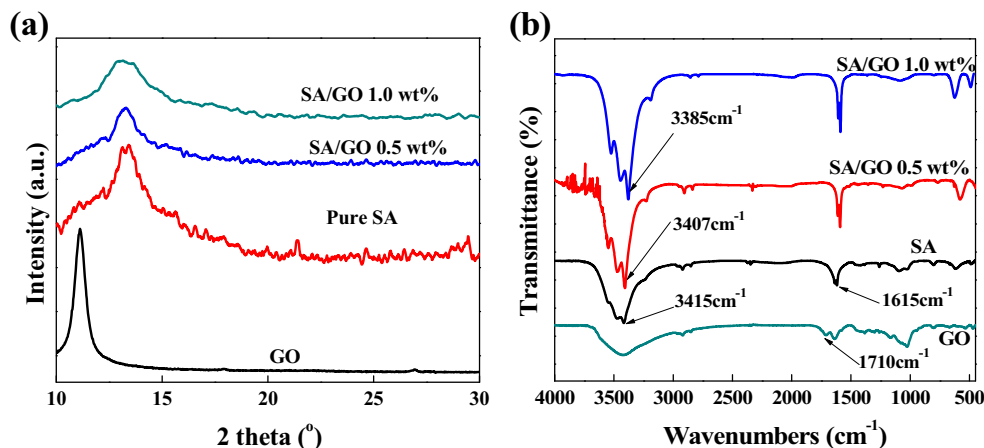
BPA adsorption of the hydrogel beads

In a vial, 10 mg of freeze-dried hydrogel beads was put into 25 mL of BPA solution. The detailed procedures for measuring the adsorption behavior of the hydrogel beads to BPA also follow the above-mentioned method to dye solutions. The amount of the absorbed BPA by the beads was also measured by a UV-Vis spectroscopy at the wavelength of ~275 nm which represented for the π-π* transition of the phenol group.

Adsorption kinetics of hydrogel beads

Two kinetics models, the pseudo-first-order equation and the pseudo-second-order equation, are used to investigate the adsorption mechanism of the SA hydrogel beads to the dyes and BPA. The pseudo-first-order equation is shown as:

$$\ln(q_e - q_t) = \ln q_e - K_1 t \tag{4}$$

where q_t is the absorption amount (mg/g) of the dyes and BPA on the hydrogel beads at time t (h) and K_1 is the rate

constant of the pseudo-first-order adsorption (h^{-1}) [24]. The pseudo-second-order equation is shown as:

$$\frac{t}{q_t} = \frac{1}{K_2 q_e^2} + \frac{1}{q_e} t \tag{5}$$

where K_2 is the rate constant of the pseudo-second-order adsorption (mg g^{-1} h^{-1}).

Results and discussion

The XRD patterns of the pure SA hydrogel beads and SA/GO hydrogel beads are shown in Fig. 1a. As could be seen, GO exhibited characteristic peaks at ~11°, while the SA hydrogel beads had the characteristic peak at ~13.2°. When the GO was incorporated into the hydrogel beads, the composite beads presented similar peaks to the pure hydrogel, and neither GO peak nor other peaks were observed, indicating that GO sheets have been well exfoliated within the SA matrix, and the incorporation of GO did not break the pristine structure of the SA. Moreover, it could be also observed that the peak intensity of the SA/GO hydrogel beads was broader and weaker than that of the pure SA, and the SA/GO peak had a slight shift to lower value, which meant the rigid filler GO might decrease
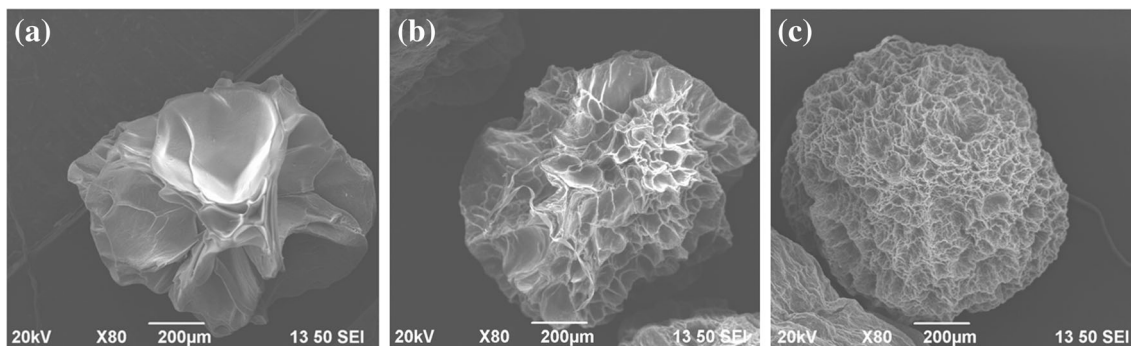

Fig. 2 SEM images of (a) SA, (b) SA/GO 0.5 wt% and SA/GO 1.0 wt% hydrogel beads
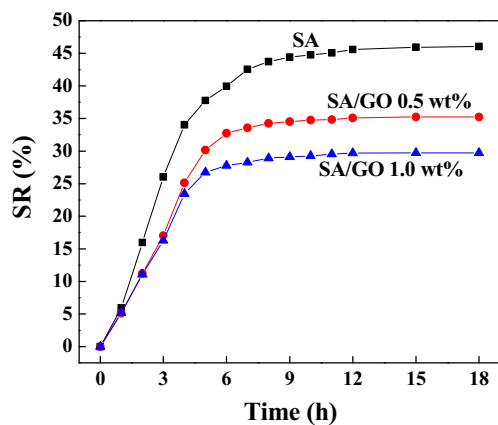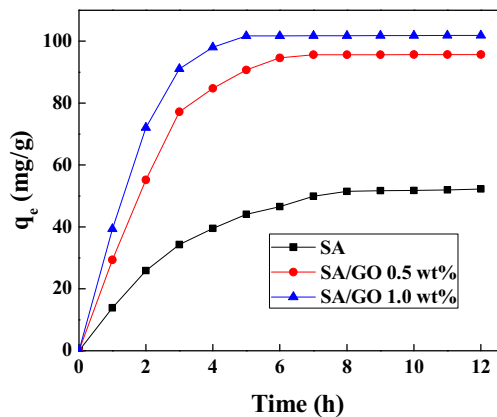
Fig. 3 The swelling behavior of the SA and SA/GO hydrogel beads

Fig. 5 Effect of GO content and contact time on the adsorption of BPA by SA and SA/GO hydrogel beads at room temperature (25 °C) and pH value at 7.0

the crystallinity of the polymer matrix to some extent when the filler was incorporated and interacted with the matrix [25].

Figure 1b shows the FT-IR spectra of the GO, SA, and SA/GO hydrogel beads. It can be seen that GO had characteristic peaks at 1710 and ~3300 cm^{-1}, which were corresponded to the stretching vibration of the –OH group and the –COOH groups on the GO surface. These groups were the functional groups which could form interactions with the SA molecules and the adsorbed targets. The pure SA had characteristic peaks at ~3415 and ~1615 cm^{-1}, which were attributed to the stretching vibration of the –

OH group and the C=O group in the SA molecules. From the spectra of the SA/GO hydrogel beads, GO peak could be observed due to low incorporation content. Meanwhile, it could be seen that the vibration peak of the –OH group became broader with lower wavelengths, indicating the SA matrix and the GO filler had some sort of interactions through hydrogen bonding. Moreover, with the increase of the GO content in the hydrogel, a bigger shifting degree was observed, indicating more hydrogen bond inter-

Fig. 4 Effect of GO content and contact time on the adsorption of (**a**) MB, (**b**) RhB, (**c**) VG1, and (**d**) MO by SA and SA/GO hydrogel beads at room temperature (25 °C) and pH value at 7.0 (inset: digital image of the dye solutions before and after adsorption: 1. Before adsorption; 2. Adsorption by SA; 3. Adsorption by SA/GO)
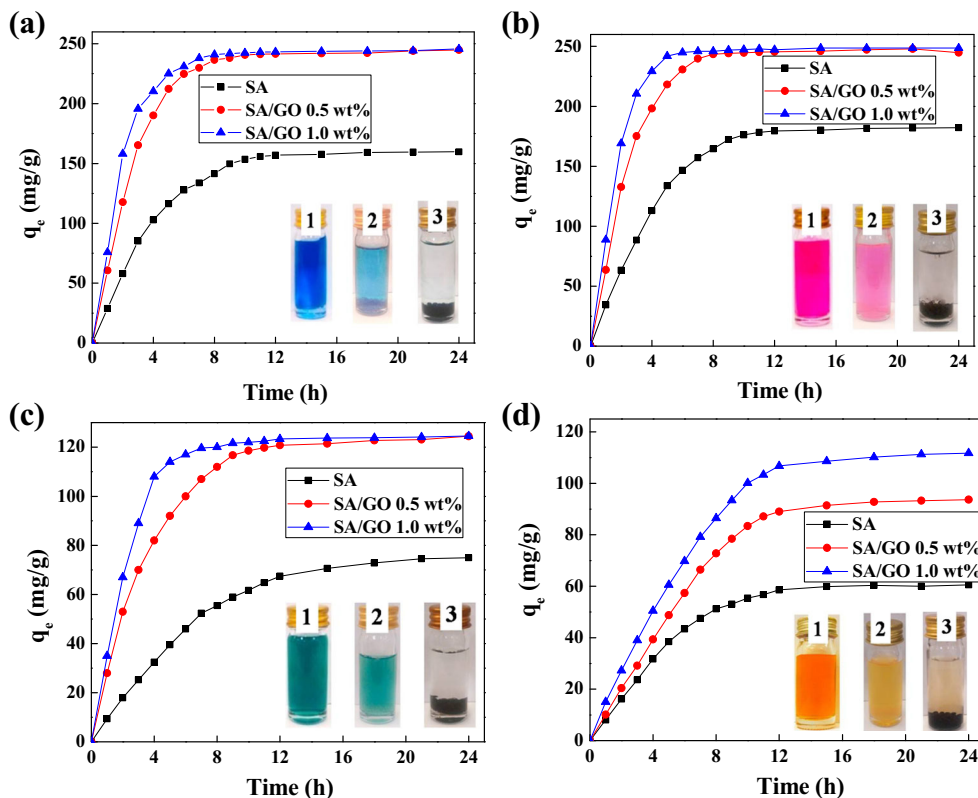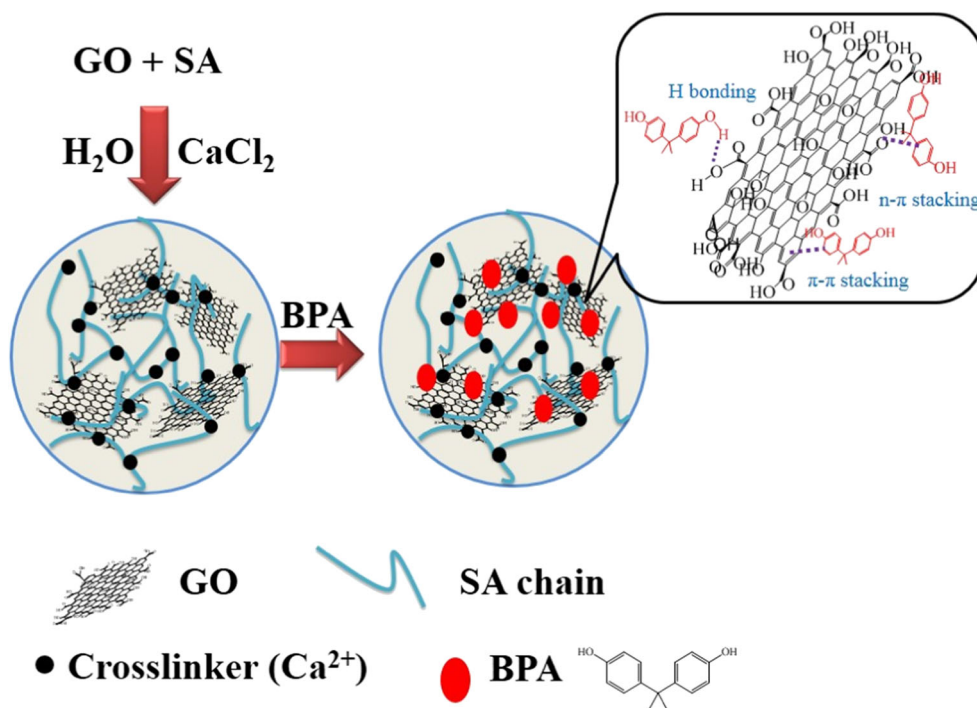
actions were formed. Meanwhile, the peak intensity of the SA/GO hydrogel beads in ~1615 cm^{-1} was higher than that of the pure SA hydrogel beads, which also meant the SA and GO formed strong interactions.

Figure 2 shows the SEM image of the freeze-dried pure SA and SA/GO hydrogel beads. It could be seen that both the SA and SA/GO hydrogel beads had well-defined porous structure. However, it could be seen that the pore size of the SA/GO hydrogel was smaller than that of the SA hydrogel. The more GO was incorporated into the SA, the smaller the pore size of the hydrogel beads. This was ascribed to the introduction of the GO in to the hydrogel system who brought about a number of functional groups like –OH groups and –COOH groups.

These functional groups took part in the crosslinking process and formed strong hydrogen bonding interactions with the SA as described above, resulting in a higher crosslinking degree and a smaller pore size [26].

The crosslinking of the GO also affected the swelling behavior of the prepared hydrogel beads. Figure 3 shows the water holding capacity in terms of swelling ratio of the hydrogel beads. One can see that with the incorporation of the GO, the SR of the SA/GO hydrogel beads when compared with the pure SA beads. Since the functional groups in GO increased the crosslinking degree of the hydrogel beads, the interactions between the SA and the water molecules were interfered and restrained, resulting in a lower degree on the SR of the SA/GO hydrogel beads [27].

The adsorption capability of the hydrogel beads to various organic dyes was then investigated. Figure 4 shows the influence of the contact time and GO mass content on the dyes adsorbed on the hydrogel beads at room temperature (25 °C) and pH value at 7.0. The inset images were the color changes before and after adsorption. As could be clearly observed, the existence of the GO significantly enhanced the dye adsorption capability of the dyes and almost all the dyes could be effectively adsorbed within 8 h of time. This was ascribed to the large aromatic structure and the existence of numerous functional groups of the GO which could easily capture the dye molecules through π-π stacking and ionic interactions. It could be also seen that the adsorption speed of the MO onto the hydrogel beads
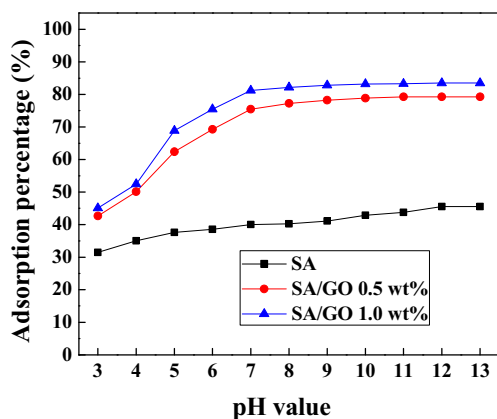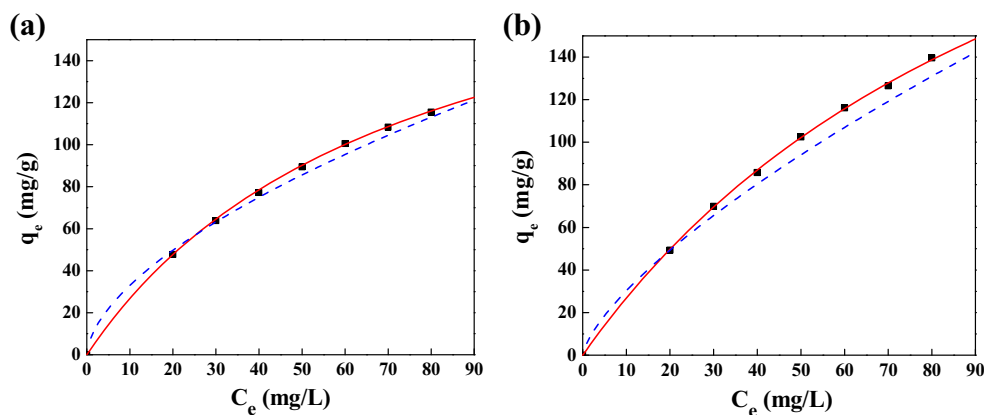

Fig. 7 Influence of pH value on BPA adsorption by the hydrogel beads

Fig. 8 Adsorption isotherms of (**a**) SA/GO 0.5 wt% and (**b**) SA/GO 1.0 wt% hydrogel beads to BPA including experimental data (black dot); Langmuir model (red solid line), and Freundlich model (blue dash line)

was slower than those of the MB, RhB, and VG1. Since GO had numerous carboxyl functional groups within its structure and can be easily negatively charged in water (COOH→COO⁻ + H⁺), the positively charged and neutral dye molecules like MB, RhB, and VG1 are more inclined to be adsorbed by the negatively charged MO (see Table 1), which resulted in a better adsorption of the MB, RhB, and VG1 [28]. Li et al. [29] studied the adsorption behavior of SA/GO fiber film to MB and found that the SA/GO composite had an adsorption capacity of 140.80 mg/g to MB. When the shape of the SA/GO composite changed to beads in the present study, the adsorption capacity to MB could be higher than 200 mg/g due to larger contact areas.

The adsorption of the hydrogel beads to BPA was then investigated in detail. Figure 5 shows the influence of the contact time and GO mass content on the BPA adsorbed on the hydrogel beads at room temperature (25 °C) and pH value at 7.0. The BPA concentration was set at 50 mg/L. The results showed that the SA/GO beads had very desirable removal efficiency to the BPA, in which a larger amount of the BPA molecules could be adsorbed by the hydrogel beads within 6 h of time. On the contrary, the pure SA hydrogel beads showed a poor adsorption capacity of ~ 50 mg/g. This was also due to the existence of the

GO which increased the interactions with the benzene rings within the BPA structure through π-π stacking, n-π stacking, and hydrogen bonding (see Fig. 6), which was in accordance with the previous studies [30].

Successively, the influence of the pH value on the adsorption behavior of the hydrogel beads to BPA was studied since the hydrogen/hydroxide ion concentrations affected the surface charges and properties of the GO and SA a lot. Figure 7 shows the adsorption of the hydrogel beads to BPA at different pH value. One could see that the total BPA adsorption amount increased with the increase of the pH value. At lower pH, the successive protons (H⁺) integrated with the carboxyl groups (COO⁻) of the GO, hindering the n-π stacking and hydrogen bonding interactions between the hydrogels and BPA molecules. When the pH value increased, the GO surface was negatively charged in which more carboxyl groups could take part in the interactions, and the BPA adsorption amount was then increased as a result. Since the introduction of the GO into the hydrogel system brought about abundant carboxylic acid groups, a more obvious adsorption variation could be observed on the SA/GO hydrogel beads [31].

The adsorption isotherm of BPA on the SA/GO hydrogel beads was then investigated with the results shown in Fig. 8a, b. Ten milligrams of the SA/GO 0.5 wt% and SA/GO 1.0 wt% were selected as the adsorbent to be put into 25 mL of BPA solution, and the BPA concentration increased from 20 to 80 mg/L. The BPA adsorption data were fitted by the Langmuir model and Freundlich model as follows:

$$q_e = \frac{q_m K_L C_e}{1 + K_L C_e} \tag{5}$$

where q_m is the theoretical maximal adsorption amount when monolayer absorbent is fully covered with the absorbate (mg/

Table 2 Isotherms parameters for SA/GO hydrogel beads

Isotherm model	Parameters	SA/GO 0.5 wt%	SA/GO 1.0 wt%
Langmuir	q_m (mg/g)	221.92	342.69
	K_L (L/mg)	0.0137	0.00851
	R^2	0.996	0.993
Freundlich	K_f (L/g)	8.43	5.98
	n	1.688	1.421
	R^2	0.955	0.938
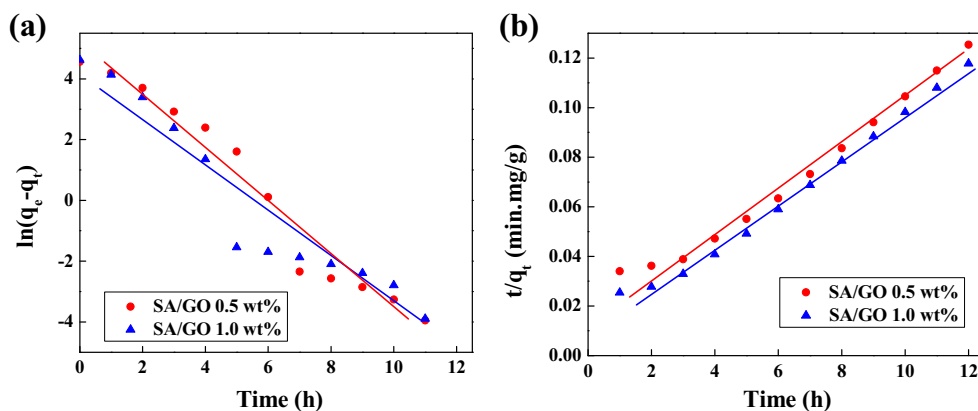
g) and K_L is the Langmuir constant (L/g) which relates to the adsorption energy.

$$\ln q_e = \ln K_f + \frac{1}{n}\ln C_e \tag{6}$$

where K_f is the Freundlich constant (mg/g) which related to the adsorption capacity and $\frac{1}{n}$ is also a Freundlich constant which related to the adsorption intensity. The detailed parameters are also listed in Table 2.

As could be observed, for both SA/GO 0.5 wt% and SA/GO 1.0 wt% hydrogel beads, the obtained data can be fitted for both the Langmuir model and Freundlich model as well. From the R^2 values shown in Table 2, one could see that the Langmuir model ($R^2 \approx 0.99$) illustrates better correlation than the Freundlich model ($R^2 \approx 0.94$), indicating a homogeneous surface of the hydrogel beads and a uniform adsorption of the BPA on the adsorbent samples.

The adsorption kinetics was also investigated and analyzed with pseudo-first-order and pseudo-second-order models. Figure 9a, b shows the adsorption kinetic results of the SA/GO 0.5 wt% and SA/GO 1.0 wt% hydrogel beads. It could be clearly seen that the time and t/q_t had a linear relationship in pseudo-second-order model for both two hydrogel bead samples. However, nonlinear relationship between the time and $\ln(q_e - q_t)$ was observed in pseudo-first-order model. The results indicated that the experimental data agreed with the calculated values well and the adsorption behaviors in the present study obeyed the pseudo-second-order model.

Conclusion

In summary, the SA/GO hydrogel beads with different GO mass contents were prepared through a facile ion exchange process. The prepared hydrogel beads were used to remove organic pollutants like various dyes and BPA in aqueous media. The overall results showed that the prepared SA/GO hydrogel beads had very promising adsorption capabilities to the

mentioned pollutants. The incorporation of the GO largely enhanced and increased the adsorption amount of the SA hydrogel beads. Afterwards, the adsorption isotherms and kinetics of the SA/GO hydrogel beads to BPA were also investigated in detail, and the results show the adsorption behavior follows the Langmuir model and pseudo-second-order model well. This study provides an effective and efficient absorbency for potential applications in removing pollutants in water purification fields.

Compliance with ethical standards

Conflict of interest The authors declare that they have no conflict of interest.

References

1. Ma L, Wen J (2008) Biocomposite of double-walled carbon nanotube-doped alginate gel for biomaterial immobilization. Compos Sci Technol 68(6):1297–1303. https://doi.org/10.1016/j.compscitech.2007.12.009

2. Mookhoek SD, Fischer HR, van der Zwaag S (2012) Alginate fibres containing discrete liquid filled vacuoles for controlled delivery of healing agents in fibre reinforced composites. Compos A Appl Sci 43(12):2176–2182. https://doi.org/10.1016/j.compositesa.2012.08.006

3. Zhang H, Zhang Y, He L, Yang B, Zhu S, Yao M (2016) Thermal-responsive poly(N-isopropyl acrylamide)/sodium alginate hydrogels: preparation, swelling behaviors, and mechanical properties. Colloid Polym Sci 294(12):1959–1967. https://doi.org/10.1007/s00396-016-3951-2

4. Gan L, Xu LJ, Pan ZP, Jiang FY, Shang SM (2016) Alginic acid/graphene oxide hydrogel film coated functional cotton fabric for

controlled release of matrine and oxymatrine. RSC Adv 6(80): 76420–76425. https://doi.org/10.1039/C6RA15543J

5. Han F, Dong Y, Song A, Yin R, Li S (2014) Alginate/chitosan based bi-layer composite membrane as potential sustained-release wound dressing containing ciprofloxacin hydrochloride. Appl Surf Sci 311:626–634. https://doi.org/10.1016/j.apsusc.2014.05.125

6. Seo HJ, Kim JC (2015) In situ preparation of gold nanospheres in bead composed of alginate/poly(N-isopropylacrylamide-co-di-methyl aminoethyl methacrylate) and photothermal controlled release. Colloid Polym Sci 293(5):1425–1435. https://doi.org/10.1007/s00396-015-3524-9

7. Zhang Y, Lin X, Hu S, Zhang X, Luo X (2016) Core-shell zeolite@Alg-Ca particles for removal of strontium from aqueous solutions. RSC Adv 6(78):73959–73973. https://doi.org/10.1039/C6RA11112B

8. Li Z, Jiang W, Zhang L, Wang Y, Wei G (2015) Adsorption of cationic dye from water using thermo-sensitive colloid composed of methylcellulose and sodium alginate. Colloid Polym Sci 293(10):2753–2761. https://doi.org/10.1007/s00396-015-3666-9

9. Gan L, Shang SM, Yuen CWM, Jiang SX (2015) Graphene nanoribbon coated flexible and conductive cotton fabric. Compos Sci Technol 117:208–214. https://doi.org/10.1016/j.compscitech.2015.06.019

10. Gan L, Shang SM, Yuen CWM, Jiang SX (2015) Covalently functionalized graphene with d-glucose and its reinforcement to poly(-vinyl alcohol) and poly(methyl methacrylate). RSC Adv 5(21): 15954–15961. https://doi.org/10.1039/C5RA00038F

11. Gan L, Shang S, Hu E, Yuen CWM, Jiang SX (2015) Konjac glucomannan/graphene oxide hydrogel with enhanced dyes adsorption capability for methyl blue and methyl orange. Appl Surf Sci 357(Part A):866–872. https://doi.org/10.1016/j.apsusc.2015.09.106

12. Tan L, Gan L, Hu J, Zhu Y, Han J (2015) Functional shape memory composite nanofibers with graphene oxide filler. Compos A Appl Sci 76:115–123. https://doi.org/10.1016/j.compositesa.2015.04.015

13. Gan L, Xu LJ, Shang SM, Zhou XY, Meng L (2016) Visible light induced methylene blue dye degradation photo-catalyzed by WO3/graphene nanocomposites and the mechanism. Ceram Int 42(14): 15235–15241. https://doi.org/10.1016/j.ceramint.2016.06.160

14. Kumar R, Singh RK, Singh DP, Savu R, Moshkalev SA (2016) Microwave heating time dependent synthesis of various dimensional graphene oxide supported hierarchical ZnO nanostructures and its photoluminescence studies. Mater Des 111:291–300. https://doi.org/10.1016/j.matdes.2016.09.018

15. Zhang ZY, Xiao F, Guo YL, Wang S, Liu YQ (2013) One-pot self-assembled three-dimensional TiO2-graphene hydrogel with improved adsorption capacities and photocatalytic and electrochemical activities. ACS Appl Mater Interfaces 5(6):2227–2233. https://doi.org/10.1021/am303299r

16. Wang X, Liu Z, Ye X, Hu K, Zhong H, Yu J, Jin M, Guo Z (2014) A facile one-step approach to functionalized graphene oxide-based hydrogels used as effective adsorbents toward anionic dyes. Appl Surf Sci 308:82–90. https://doi.org/10.1016/j.apsusc.2014.04.103

17. Gan L, Xu LJ, Qian K (2016) Preparation of core-shell structured CoFe2O4 incorporated Ag3PO4 nanocomposites for photocatalytic degradation of organic dyes. Mater Des 109:354–360. https://doi.org/10.1016/j.matdes.2016.07.043

18. Tang L, Xie Z, Zeng G, Dong H, Fan C, Zhou Y, Wang J, Deng Y, Wang J, Wei X (2016) Removal of bisphenol A by iron

nanoparticle-doped magnetic ordered mesoporous carbon. RSC Adv 6(31):25724–25732. https://doi.org/10.1039/C5RA27710H

19. Wu S, Zhao X, Li Y, Zhao C, Du Q, Sun J, Wang Y, Peng X, Xia Y, Wang Z, Xia L (2013) Adsorption of ciprofloxacin onto biocomposite fibers of graphene oxide/calcium alginate. Chem Eng J 230(Supplement C):389–395. https://doi.org/10.1016/j.cej.2013.06.072

20. Algothmi WM, Bandaru NM, Yu Y, Shapter JG, Ellis AV (2013) Alginate–graphene oxide hybrid gel beads: an efficient copper adsorbent material. J Colloid Interface Sci 397(Supplement C):32–38. https://doi.org/10.1016/j.jcis.2013.01.051

21. Jin Z, Wang X, Sun Y, Ai Y, Wang X (2015) Adsorption of 4-n-Nonylphenol and bisphenol-A on magnetic reduced graphene oxides: a combined experimental and theoretical studies. Environ Sci Technol 49(15):9168–9175. https://doi.org/10.1021/acs.est.5b02022

22. Ouyang K, Zhu C, Zhao Y, Wang L, Xie S, Wang Q (2015) Adsorption mechanism of magnetically separable Fe3O4/graphene oxide hybrids. Appl Surf Sci 355(Supplement C):562–569. https://doi.org/10.1016/j.apsusc.2015.07.109

23. Gan L, Shang S, S-x J (2016) Impact of vinyl concentration of a silicone rubber on the properties of the graphene oxide filled silicone rubber composites. Compos Part B Eng 84:294–300. https://doi.org/10.1016/j.compositesb.2015.08.073

24. Cheng C, Ma L, Ren J, Li L, Zhang G, Yang Q, Zhao C (2011) Preparation of polyethersulfone-modified sepiolite hybrid particles for the removal of environmental toxins. Chem Eng J 171(3):1132–1142. https://doi.org/10.1016/j.cej.2011.05.011

25. Gan L, Shang S, Yuen CWM, S-x J, Luo NM (2015) Facile preparation of graphene nanoribbon filled silicone rubber nanocomposite with improved thermal and mechanical properties. Compos Part B Eng 69:237–242. https://doi.org/10.1016/j.compositesb.2014.10.019

26. Zeng Y, Qiu L, Wang K, Yao J, Li D, Simon GP, Wang R, Wang H (2013) Significantly enhanced water flux in forward osmosis desalination with polymer-graphene composite hydrogels as a draw agent. RSC Adv 3(3):887–894. https://doi.org/10.1039/C2RA22173J

27. Fan Z, Liu B, Wang J, Zhang S, Lin Q, Gong P, Ma L, Yang S (2014) A novel wound dressing based on ag/graphene polymer hydrogel: effectively kill bacteria and accelerate wound healing. Adv Funct Mater 24(25):3933–3943. https://doi.org/10.1002/adfm.201304202

28. Sandeman SR, Gun'ko VM, Bakalinska OM, Howell CA, Zheng Y, Kartel MT, Phillips GJ, Mikhalovsky SV (2011) Adsorption of anionic and cationic dyes by activated carbons, PVA hydrogels, and PVA/AC composite. J Colloid Interface Sci 358(2):582–592. https://doi.org/10.1016/j.jcis.2011.02.031

29. Li Y, Du Q, Liu T, Sun J, Wang Y, Wu S, Wang Z, Xia Y, Xia L (2013) Methylene blue adsorption on graphene oxide/calcium alginate composites. Carbohydr Polym 95(1):501–507. https://doi.org/10.1016/j.carbpol.2013.01.094

30. Yang YF, Xie YL, Pang LC, Li M, Song XH, Wen JG, Zhao HY (2013) Preparation of reduced graphene oxide/poly(acrylamide) nanocomposite and its adsorption of Pb(II) and methylene blue. Langmuir 29(34):10727–10736. https://doi.org/10.1021/la401940z

31. Ai L, Jiang J (2012) Removal of methylene blue from aqueous solution with self-assembled cylindrical graphene–carbon nanotube hybrid. Chem Eng J 192(0):156–163. https://doi.org/10.1016/j.cej.2012.03.056